Ac conductivity and dielectric properties of CuFe1xCrxO2:Mg delafossite

M Lalanne, P Demont, A Barnabé

AC conductivity and dielectrics properties of $CuFe_{1-x}Cr_xO_2$:Mg delafossite

M Lalanne, P Demont and A Barnabé

Institut Carnot CIRIMAT, Université de Toulouse UPS, 118 Route de Narbonne, 31062, Toulouse cedex 9 France

E-mail :demont@cict.fr

Abstract

The electrical and dielectric properties of $CuFe_{1-x}Cr_xO_2$ ($0 \leq x \leq 1$) powders, doped with 3 % of Mg and prepared by solid-sate reaction, were studied by broadband dielectric spectroscopy in the temperature range from -100 to 150°C. The frequency-dependent electrical and dielectric data have been discussed in the framework of a power law conductivity and complex impedance and dielectric modulus. At room temperature, the ac conductivity behaviour is characteristic of the charge transport in $CuFe_{1-x}Cr_xO_2$ powders. The substitution of Fe^{3+} by Cr^{3+} results in an increase of dc conductivity and a decrease of the Cu^{+}-Cu^{+} distance. Dc conductivity, characteristic onset frequency and Havriliak-Negami characteristics relaxation times are thermally activated above -40°C for x= 0.835. The associated activation energies obtained from dc and ac conductivity and from impedance and modulus losses are similar and show that $CuFe_{1-x}Cr_xO_2$ delafossite powders satisfy the BNN relation. Dc and ac conductivities have the same transport mechanism, namely thermally activated nearest neighbour hopping and tunnelling hopping above and below -40°C respectively.

1. Introduction

For more than 30 years, delafossite compounds have been studied for their unusual magnetic and electrical properties [1-3]. More recently, delafossite compounds have attracted much attention since Kawazoe *et al*. [4] showed that $CuAlO_2$ was a good candidate for p-type transparent conducting oxides (TCO). The development of p-type TCO is one of the most crucial technologies for p-n junction-based devices such as transparent solar cells and transparent light emitting diodes. Among various materials, copper metal oxide with the molar ratio Cu/M = 1, i.e. $CuMO_2$, with M = {Al, Ga, Cr, …} and with delafossite structure has been known as one of the p-type TCO materials for potential industrial applications. Several $CuMO_2$ thin films have been reported with different conductivities and transparencies [5-9].

The $CuMO_2$ structure can be described as a stacking, along the *c* axis, of edge-shared MO_6 octahedra forming MO_2 layers. These MO_2 layers are connected together with triangular metallic planes of monovalent copper. Each Cu^+ cation is linearly coordinated with two O^{2-} anions of upper and lower MO_2 layers as seen in figure 1. The oxygen layers can be stacked in different ways along the *c* axis, leading to two polytypes of the delafossite structure: the hexagonal 2H (space groupe $P6_3/mmc$) and the rhombohedral 3R (space group R-3m) polytypes.

$CuFeO_2$ delafossite is a well-known p-type semiconductor. At room temperature, the highest electrical conductivity (σ_{RT} = 2 S.cm^{-1}) [1, 10] among the $CuMO_2$ delafossite series is obtained with p-type $CuFeO_2$ delafossite when an off-stoichiometric $CuFeO_{2+\delta}$ phase is formed. This electrical conductivity can also be improved by magnesium doping up to 30 S.cm^{-1} for $CuFe_{0.98}Mg_{0.02}O_2$ [10, 11]. In the $CuMO_2$ compounds, the transport properties are mainly governed by the copper mixed valency Cu^I/Cu^{II} [12, 13]. In $CuFeO_{2+\delta}$ and $CuFe_{1-x}Mg_xO_2$, this Cu^I/Cu^{II} ratio is respectively controlled by the oxygen non stoichiometry value δ according to $(Cu^+_{1-2\delta}Cu^{2+}_{2\delta})FeO_{2+\delta}$ [14], and the Fe-site doping stoichiometry *x* according to $(Cu^+_{1-x}Cu^{2+}_{x})$ $(Cr^{3+}_{1-x}Mg^{2+}_{x})O_2$. Moreover, $CuFeO_2$ can be deposited in thin film form by radio-frequency sputtering method at low temperature on conventional glass [15], and then accordingly presents a real interest for industrial applications.

$CuCrO_2$ delafossite is also a p-type semiconductor but with a lower intrinsic electrical conductivity (σ_{RT} = 3.5 10^{-5} S.cm^{-1}) [9] due to the difficulties in intercalating oxygen into the stoichiometric delafossite structure [16]. However, the electrical conductivity can be also improved up to 220 S.cm^{-1} with appropriate M-site doping like in $CuCr_{0.95}Mg_{0.05}O_2$ thin film [8], by the same way than $CuFeO_2$.

As a result, $CuFe_{1-x}Cr_xO_2$:Mg solid solution is particularly attractive due to the potential merge of the low temperature deposition process of the p-type $CuFeO_2$ delafossite and the optimized p-type TCO properties of $CuCrO_2$:Mg.

Previously, we studied the phase stability and thermal behaviour of the $CuFe_{1-x}Cr_xO_2$ ($0 \leq x \leq 1$) solid solution by thermogravimetric analysis (TGA) and high-temperature XRD under an air

atmosphere up to 1000°C in order to characterize the oxygen intercalation [16]. For $0 \leq x < 1$, two oxidations were observed. A slight oxidation appears between 400 and 500°C, leading oxygen intercalation in the Cu^{+} layers. An off-stoichiometric $(Cu^{+}_{1-2\delta}Cu^{2+}_{2\delta})Fe_{1-x}Cr_xO_{2+\delta}$ delafossite phase is then formed. Above 500°C, a phase transition occurs; the delafossite phase is transformed into spinel and CuO phases. For $x = 1$, i.e.$CuCrO_2$, the delafossite phase is thermally stable in air up to 1000°C.

In this paper, the electrical properties of $CuFe_{1-x}Cr_xO_2$:Mg ($0 \leq x \leq 1$) solid solutions were studied by dielectric spectroscopy in order to observe the effect of the substitution of Fe by Cr on the M-site on the electrical conduction mechanism.

2. Experimental section

Polycrystalline samples of $CuFe_{1-x}Cr_xO_2$ ($0 \leq x \leq 1$) doped with 3 % of Mg were prepared by a conventional solid-state reaction from stoichiometric mixtures of Cu_2O, Fe_2O_3, Cr_2O_3 and MgO commercial powders. Mg content is fixed to 3 % in order to avoid the precipitation of the secondary phases [17].The obtained mixtures were heated in a nitrogen atmosphere between 900 and 1000°C for 30 h with intermittent grindings. Then, the powders were pressed into pellets and sintered at 1050°C in neutral atmosphere for 10 h.

Electrical conductivity measurements were performed by recording the complex impedance $Z^*(\omega)$ and complex conductivity $\sigma^*(\omega)$ using a Novocontrol broadband dielectric spectrometer. The measurements were done in the frequency range from 10^{-2} to 10^{6} Hz at room temperature and in the temperature range from -100 to 150°C. The real part, $\sigma'(\omega)$, of the complex conductivity was investigated. The ac output voltage was adjusted to 1.5 V. For all the samples considered in this study, the phase lag between the measured impedance and the applied ac voltage was negligible at low frequencies, so that the reported impedance at 0.01 Hz is equivalent to the dc resistance. The dc conductivity σ_{dc} of samples was determined from the independent frequency part of $\sigma'(\omega)$ (low frequency plateau).

The powder samples were enclosed in a Teflon sample holder between two circular stainless steel electrodes (10 mm in diameter). The sintered samples 1.6 mm thick were placed between two circular gold platted electrodes (10 mm in diameter). To reduce contact resistance with the cell electrodes, a thin layer of gold (100 nm) was sputtered onto both sides of the pellets using a BOC Edwards scancoat six SEM sputter coater.

3. Results and Discussion

3.1. *DC and AC conductivity*

Figure 2 shows the frequency dependence of the real part, $\sigma'(\omega)$ of the complex electrical conductivity, for Mg-doped $CuFe_{1-x}Cr_xO_2$ powders at room temperature (25°C°). At low frequencies, $\sigma'(\omega)$ is independent of the electric field frequency. Above a characteristic onset angular frequency ω_c, the ac conductivity increases with increasing angular frequency and obeys a power law. Then, the angular frequency dependence of the total ac conductivity is well described by the following equation:

$$\sigma'(\omega) = \sigma(0) + A\omega^n = \sigma_{dc}\,[1 + (\frac{\omega}{\omega_c})^n] \qquad (1)$$

where σ_{dc} is the independent frequency conductivity or dc conductivity, $A = \omega_c^{-n}\,\sigma_{dc}$ is a pre-exponential factor and n is an exponent dependent on both frequency and temperature in the range $0 < n \leq 1$. This behaviour is characteristics of the charge transport in disordered materials and interpreted by Jonscher [18] as universal dynamic response (UDR). However a value of n >1 was reported in ion-conducting glasses [19], ionic crystals [20-21] and underlined by Papathanassiou *et al* [22-23] in a new approach of the universal power law in disordered materials. The experimental $\sigma'(\omega)$ conductivity for $CuFe_{1-x}Cr_xO_2$ powders were fitted using (1). The best fits of the conductivity spectra at room temperature for $0 \leq x \leq 1$ are shown as solid lines in figure 2. The dc conductivity σ_{dc}, the crossover frequency ω_c and the exponent n were obtained by a non-linear fitting procedure and reported in table 1. The variation of the dc conductivity with x is shown in figure 3. As expected the conductivity increases weakly with x, only one decade in magnitude, because the progressive substitution of Fe^{3+} by Cr^{3+} reduces the distance Cu^+-Cu^+ in $CuFe_{1-x}Cr_xO_2$. The inset in figure 3 shows the variation of the power law exponent n with x. The exponent n decreases from 0.92 for $CuFeO_2$ (x=0) to 0.65 for $CuCrO_2$ (x=1) and a sharp decrease is observed above x=0.5. This behaviour can be compared with the decrease of particles sizes of $CuFe_{1-x}Cr_xO_2$ solid solution with increasing x [16]. The substitution of Fe^{3+} by Cr^{3+} leaded to contraction of unit cell, and reduction of lattice parameter a. The lower value of n above x= 0.5 indicates that the dispersion of ac conductivity with frequency is reduced with the introduction of large amount of Cr at Fe site. This behaviour may be correlated with the change in the

distance and barrier height of the sites available for charge carriers for electrical conduction. The decrease of the lattice parameter *a* in the plane of the Cu atoms and the increased overlap between $Cu^{+}(3d^{10})$ with increasing *x* are responsible of the observed *n* decrease through a reinforcement of the interaction between Cu^{+} ions.

The ac conductivity is dependent of the stoichiometric parameter *x* as the dc conductivity and don't obey a scaling with *x*, i.e., no scaling law is obtained for all the $CuFe_{1-x}Cr_xO_2$ delafossite when the reduced conductivity $\sigma'(\omega)/\sigma_{dc}$ is plotted against the reduced frequency $\omega_r=a_x\omega$ where $a_x=[\omega(x)/\omega(x=1)]$ is a shit factor depending on *x*, i.e., all the conductivity curves at constant *x* don't fall onto one master curve. The shape of the frequency dependence of the ac conductivity is then dependent of *x* as dc conductivity and the onset frequency.

According to the revision of the universal power law dispersion of ac conductivity in disordered solids proposed by Papathanassiou [22], the ratio $-LnA/n$ is reported as a function of *x* in figure 4. This ratio is near constant because the weak change in the dc conductivity value with the substitution of Fe^{3+} by Cr^{3+}. Such behaviour, i.e., $-LnA/n$ independent of composition, was observed in ion-conducting glasses [19].

The effect of Cr substitution on the conduction relaxation mechanism of $CuFe_{1-x}Cr_xO_2$ powder were also investigated by the complex impedance $Z^*(\omega)$ and complex dielectric modulus $M^*(\omega)$ as the function of angular frequency and temperature. Electrical modulus formalism was used in conductive materials to distinguish a frequency domain within the charge transport is long range and above which is localized since it emphasizes bulk properties compared with the interfacial polarization. The frequency dependence of the imaginary part' of $Z^*(\omega)$, $Z''(\omega)$ is shown in figure 5 for $CuFeO_2$ (x=0) to and $CuCrO_2$ (x=1) and compared with the $\sigma'(\omega)$ behaviour. The relaxation conduction of charge carriers is represented by well-defined loss peaks in $Z''(\omega)$ and no such corresponding peak in the imaginary part of the complex dielectric permittivity $\varepsilon''(\omega)$ occurs. The maximum of the *Z"* spectrum, occurring in the high frequency range part of the experimental frequency range [10^{-2}-10^{6} Hz], is associated to the contribution of the bulk property of the material. Let τ_Z be the relaxation times obtained from impedance plot. The absence of a ε'' loss peak together with the equivalence $\omega_c^{-1} \approx \tau_Z$

signify long range charge carriers diffusion. The conduction relaxation mechanism in $CuFe_{1-x}Cr_xO_2$ powder is also investigated by analyzing electrical loss modulus *M"* as a function of frequency and temperature. Imaginary part of modulus spectra is reported in figure 6 for *x*=0 to and *x*=1 and compared with *Z"* spectra. The *M''* spectrum exhibits one main peak as the *Z''* spectrum. It is important to note that *M"* maxima are at higher frequency in respect to *Z''* maxima. Let τ_M be the relaxation times obtained from modulus plot. The relatively large width and asymmetrical nature of the *Z"* and *M''* peaks at room temperature indicate a non-Debye behaviour of the conduction relaxation process. In order to follow the effect of the substitution of Fe^{3+} by Cr^{3+} on relaxation times, Havriliak-Negami (HN) empirical equation was used to describe the frequency dependence of the shape of the *Z"* and *M''* peaks as follows:

$$Z_s^* = Z_s^{'} - i\,Z_s^{''} = \frac{R_s}{[1+(i\omega\tau_Z^*)^{\alpha}]^{\beta}} \qquad (2)$$

$$M^* = M'+i\,M'' = M_{\infty} - \frac{(M_{\infty}-M_0)}{[1+(i\omega\tau_M^*)^{\alpha}]^{\beta}} \qquad (3)$$

where τ^*_Z and τ^*_M are the (HN) characteristics relaxation time, and α and β the parameters describing the distribution of relaxation time. The parameters describing the conduction relaxation for the different $CuFe_{1-x}Cr_xO_2$ samples are listed in table 2. The variation of ω_c^{-1}, τ^*_Z and τ^*_M with *x* at room temperature is reported in figure 3. The three representations of the conduction relaxation show that the characteristics relaxation time decreases with increasing *x*. The magnitude of *Z''* is founded to decrease as *x* increases, because R_s decreases. This result is in good agreement with the shortening of the distance between Cu sites as *x* increases.

The frequency behaviour of the ac conductivity at different temperatures for *x*=0.835 is reported in figure 7. As expected for semiconductor behaviour, σ_{dc} increases with increasing temperature. Figure 8 displays the temperature dependence of the dc conductivity data in an Arrhenius plot for *x*=0.835. The activation energy for the thermally activated conduction process is obtained by fitting the dc conductivity data with the Arrhenius relation: $\sigma_{dc} = \sigma_0 \exp(-\frac{E_\sigma}{k_B T})$ (4)

where σ_0 is the pre-exponential factor, E_σ is the activation energy for dc conductivity. As can be seen, only the data from -30°C to about 150°C can be well linearized in this representation with E_σ = 0.43 eV and σ_0=1905 S.cm^{-1}.

In the universal dynamic response (UDR) the onset frequency or the crossover frequency ω_c from the dc regime at low frequencies to the dispersive regime is also the hopping frequency ω_h. The frequency behaviour of ac conductivity as a power law were largely observed in many other low mobility oxides amorphous semiconductors and disordered systems and attributed to the hopping of charge carriers between sites having variable heights and separation distances. To correlate dc and ac conductivities, the temperature dependence of the hopping frequency ω_h is compared with the corresponding dc conductivity behaviour in figure 8. As expected the crossover frequency is also thermally activated and ω_h obeys an Arrhenius equation:

$$\omega_c \equiv \omega_h = \omega_{h0} \exp(-\frac{E_h}{k_B T}) \qquad (5)$$

with an activation energy value E_h = 0.36 eV close to the value of E_σ. The value of the corresponding characteristic hopping attempt frequency $\omega_{h0} = 10^{13}$ s^{-1} is close to the lattice phonon frequency like the inverse preexponential factor $1/\tau_{0Z,M}$. It is well known that, in most conductive materials, σ_{dc} and ω_h satisfy the Barton-Nakajima-Namikawa (BNN) relation [24-26], i.e., $\sigma_{dc} = p\, \varepsilon_0\, \Delta\varepsilon\, \omega_c$ (6)

where p is a constant of order 1, $\Delta\varepsilon$ is the dielectric strength and ε_o is the permittivity of free space. σ_{dc} and ω_h are thermally activated with nearly the same activation energy. The inset in figure 5 shows the log σ_{dc} versus log ω_h for x= 0.5. The solid line is the least-squares straight-line fit and gives a slope of 1.16 close to unity in good agreement with the BNN relation $\sigma_{dc} \sim \omega_h$. It can be conclude that dc and ac conductions are correlated with each other in $CuFe_{1-x}Cr_xO_2$ delafossite and that they are governed by the same transport mechanism, namely thermally activated nearest neighbour hopping.

At the lower temperature range, below -40°C, the dc conductivity is independent of the temperature. The thermally activated behaviour for conduction in the temperature range [-30, 150°C] is confirmed by analyzing the temperature dependence of τ^*_Z and τ^*_M. It is clear that the relaxation

times predicted by each empirical equations show an activated behaviour, i.e., obey the Arrhenius equation:

$$\tau^*_{z,M} = \tau_{0Z,M}\ exp(\frac{E_{aZ,M}}{k_B T}) \quad (7)$$

where E_a is the activation energy and τ_0 is the high-temperature limit of the relaxation time. The best fit to (7) gives E_{aZ} =0.35 eV and E_{aM} =0.39 eV which corresponds to the value of dc conduction activation energy E_σ. This result indicates that charge carrier has to overcome the same energy barrier while conducting as well as relaxing. The mechanism of electrical conduction is the same as that of dielectric relaxation in $CuFe_{1-x}Cr_xO_2$ powder. As expected from the observed dc conductivity temperature behaviour, ω_c and τ^*_Z are independent of the temperature below -40°C.

In hopping transport, we can use the relationship between the dc conductivity σ_{dc} and the hopping frequency ω_h [22],

$$\sigma_{dc} = (\frac{N_c e^2 r_h^2}{12\pi k_B T})\omega_h \quad (8)$$

where r_h is the hopping distance (i.e., the Cu-Cu distance a [16]) and N_c is the number density of effective charge carrier. Using (8), N_c can be evaluated at room temperature and compared to the number density of Cu sites in $CuFe_{1-x}Cr_xO_2$ delafossite. As shown in table 2, N_c increases with x and the value is close to N_{Cu} for $CuCrO_2$ (x=1). As expected N_c is if one take into account that the charge carrier hopping probability is necessarily reduced to some extent in the real delafossite powder. From σ_{dc} and N_c, the charge carrier mobility μ can be obtained using $\mu = \frac{\sigma_{dc}}{e N_c}$ (9) and is reported in table 2.

To complete the temperature behaviour of ac conductivity, the temperature dependence of the frequency exponent n for x= 0.835 is shown in the figure 9. The value of n calculated from (1) in figure 10 is decreasing with increasing temperature from -30 to 50°C and is increasing above 80°C. The temperature dependence of n, at low temperature up to -10°C, is weak compared with the variation above 0°C. This behaviour suggests that relaxation processes and conduction mechanism at low temperature are linked to tunnelling of charge carriers. This result is in agreement with the weak activation energy measured below -40°C using the temperature dependence of dc conductivity; impedance and loss modulus (see figures 8 and 9).

According to Dyre *et al* [27] presentation of a review on ac hopping conduction, the temperature dependence of the parameter n was explained on the basis of the many body interaction models. At low temperatures the interaction between the neighbouring charge carriers is almost negligible. As the

temperature increases, the interaction increases, leading to a decrease in *n*. The universal power law dependence of ac conductivity on the frequency corresponds to the short range hopping of charge carriers between the sites separated by energy barriers of varied heights. If hopping takes place between a random distribution of localized charge states, then lies between 0.5 and 1 as observed in $CuFe_{1-x}Cr_xO_2$ delafossite. The lower value of *n* occurs for multiple hops while the higher value occurs for single hops. Theoretical models have been proposed to correlate the conduction mechanism of ac conductivity with $n(T)$ behaviour. If *n* increases with temperature, a small polaron is the predominant mechanism, while the correlated barrier hopping (CBH) is characterized by a decrease of *n* with temperature [28]. Benko *et al* [2] assumed conduction mechanism by hopping of small polarons localized on the Cu sites in Mg-doped $CuFeO_2$. Substituting Mg^{2+} for Fe^{3+} by Mg doping results in the mixed valence $Cu^{+}/Cu^{2+}$and contributes a hole. The calculated carrier mobility is very low and insufficient to measure the Seebeck coefficient in sample powders and to display some precise information about the nature of the involved charge carrier in the conduction of the $CuFe_{1-x}Cr_xO_2$ delafossite.

According to Papathanassiou [22] the ratio (LnA/n), in disordered solids, is independent of the temperature. The ratio $-LnA/n$ is reported as a function of temperature in the inset of figure 4. The variation of (-LnA/n) in delafossite (x=0.835) is less than 2 orders of magnitude in the investigated temperature range. This behaviour is in agreement with those observed in other experimental data from ionic conducting glasses or disordered semiconductors and compiled by Papathanassiou [22].

From literature, the conduction mechanism in $CuCrO_2$ [8, 29-30] or $CuFeO_2$ delafossites at low temperature (T<25°C) is a hopping of holes between the nearest neighbour Cu sites in Cu layers and a crossover from thermal activation behaviour to that of 3D VRH occurs at a very low temperature. As shown in figures 8 and 9, a such VRH behaviour of σ_{dc} in $T^{0.25}$ is not observed because σ_{dc} , τ^*_Z and ω_c are independent of the temperature below -40°C. Hence the charge carrier transport occurs via tunnelling from Cu atom to another at low temperature.

4. Conclusion

The electrical conductivity and dielectric behaviour of Mg-doped $CuFe_{1-x}Cr_xO_2$ delafossite powders has been studied by dielectric spectrometry. At room temperature, the conductivity behaviour is frequency and composition dependent and obeys a power law, above the onset frequency ω_c. In $CuFe_{1-x}Cr_xO_2$ delafossite no scaling of ac conductivity has been observed at room temperature at different x. The Cu+-Cu+ distance has a great influence on electrical properties of $CuFe_{1-x}Cr_xO_2$ delafossite. The dc conductivity σ_{dc} increases with increasing x and decreasing Cu-Cu distance. The behaviour of the exponent n in the power law shows also a decrease when x increases from 0 to 1. The dc and ac conductivities are driven by the same mechanism, as the BNN relation is found to be valid. The same temperature behaviour is observed for the dc conductivity and the onset frequency: the activation energy is the same for both ac and dc conduction, confirming the BNN relation. The dielectric behaviour of $CuFe_{1-x}Cr_xO_2$ delafossite powders has been analyzed in the framework of complex impedance and complex dielectric modulus. The characteristic relaxation times τ^*_Z and τ^*_M extracted from impedance and modulus losses $Z''(\omega)$ and $M''(\omega)$, using a Havriliak-Negami empirical equation, are decreasing monotonous functions of x in agreement with the x dependence of dc conductivity. The observed dielectric behaviour is characteristic of a conduction relaxation of charge carriers. Above -40°C, the characteristic relaxation times τ^*_Z is thermally activated and the activation energy is close to the value obtained from dc conductivity for x=0.835. The relaxation conduction and dc conduction are governed by charge carriers hopping from Cu site to another. At low temperature, the charge transport occurs via tunnelling.

In delafossite, the ratio LnA/n extracted from the power law dispersion of the ac conductivity was found poorly dependent of composition and temperature.

References

[1] Rogers D. B., Shannon R. D., Prewitt C. T., Gillson J. L. 1971 *Inorg. Chem.* **10** 723

[2] F.A. Benko, F.P. Koffyberg 1984*J. Phys. Chem. Solids* **45** 57

[3]J. P. Doumerc, A. Wichainchai, A. Ammar, M. Pouchard, P. Hagenmuller 1986 *Mater. Res. Bull.* **21** 745

[4]H. Kawazoe, M. Yasukawa, H. Hyodo, M. Kurita, H. Yanagi, H. Hosono 1997Nature **389** 939

[5] H. Gong, Y. Wang, Y. Luo 2000 *Appl. Phys. Lett*. **76** 3959

[6] H. Yanagi, S.I. Inoue, K. Ueda, H. Kawazoe 2000 *J. Appl. Phys.* **88** 4159.

[7] M.K. Jayaraj, A.D. Draeseke, J. Tate, A.W. Sleight 2001*Thin Solid Films* **397** 244.

[8] R. Nagarajan, A.D. Draeseke, A.W. Sleight, J. Tate 2001 *J. Appl. Phys.* **89**, 8022.

[9] R. Nagarajan, N. Duan, M.K. Jayaraj, J. Li, K.A. Vanaja, A. Yokochi, A. Draeseke, J. Tate, A.W. Sleight 2001 Inter. J. Inorg. Mater. **3** 265

[10] F.A. Benko, F.P. Koffyberg 1987 J. Phys. Chem. Solids **48** 431

[11]T. Nozaki, K. Hayashi, T. Kajitani, 2008 Proceedings of the ICT 2007 26th International Conference on Thermoelectrics 168

[12] G. Thomas 1997 Nature **389** 907

[13] B. J. Ingram, T. O. Mason, R. Asahi, K. T. Park, A. J. Freeman 2001 Phys. Rev. B **64** 155114.

[14] E. Mugnier, A. Barnabé, Ph. Tailhades 2006 Solid State Ionics **177** 607

[15] A. Barnabé, E. Mugnier, L. Presmanes, Ph. Tailhades, 2006 Mater. Lett. **60** 3468

[16] M. Lalanne, A. Barnabé, F. Mathieu, Ph. Tailhades 2009 Inorg. Chem. **48** 6065

[17] P. W. Sadik, M. Ivill, V. Craciun, D. P. Norton 2009 Thin Solid Films **517** 3211

[18] A. K. Jonscher 1977 *Nature* **267** 673

[19] C. Cramer, S. Brunklaus, E. Ratai , Y. Gao 2003 **91** 26601

[20] R. H. Chen, R. Y. Yang, S. C. Shern 2002 **63** 2069

[21] B. Louati, M. Gargouri, K. Guidara, T. Mhiri 2005 J Phys Chem Solids **66** 762

[22] A. N. Papathanassiou 2005 Mater Lett **59** 1634, 2006 J Non-Cryst Solids **352** 5444

[23] A. N. Papathanassiou, I. Sakellis, J. Grammatikakis Appl Phys Lett 2007 **91** 122911

[24] J. L. Barton 1966 Verres Refract. **20** 328

[25] T. Nakajima 1972 Conf. on Electrical Insulation and Dielectric Phenomena, National Academy of Sciences, Washington DC 168

[26] H. Namikawa 1975 J. Non-Cryst. Solids **18** 173

[27] N. F. Mott, E. A. Davis 1979 *Electronic Processes in Non-crystalline Materials, Clarendon: Oxford*

[28] J. C. Dyre, T. B. Schroder 2000 Rev. Mod. Phys. **72** 873

[29] S. R. Elliot 1977 Phil. Mag. **36** 1291, 1987 Adv. Phys. **36** 135

[30] T. Okuda, N. Jufuku, S. Hidaka, N. Terada 2005 Phys. Rev. B. **72** 144403

[31] D. Li, X. Fang, Z. Deng, S. Zhou, R. Tao, W. Dong, T. Wang, Y. Zhao, G. Meng, X. Zhu 2007 J. Phys.D: Appl. Phys. **40** 4910

Figures Captions

Figure 1 : $CuMO_2$ delafossite structure

Figure 2: Angular frequency dependence of the real part σ'of the complex conductivity at room temperature (25°C) for different *x:* (!) *x*=0; (–) *x*=0.165; (7) *x*=0.333; ( ) *x*=0.5; (ν) *x*=0.667; (B) *x*=0.835; (ψ) *x*=1. The solid lines represent the fit of experimental data using (1). The inset represents the *x* dependence of exponent *n*.

Figure 3: x dependence of: (μ) dc conductivity; (ξ) characteristic relaxation time τ^*_Z from impedance plot ;(7) characteristic relaxation time τ^*_M from dielectric modulus plot; (–) reciprocal characteristic onset frequency ω_c^{-1}.

Figure 4: Composition dependence of the ratio (–LnA/n) in $CuFe_{1-x}Cr_xO_2$ delafossite at room temperature.

Figure 5: Angular frequency dependence of: the real part σ' of the complex conductivity for: (,) *x*=0; (ξ) *x*=1 and the imaginary part Z''_S of the complex impedance for: (–) *x*=0; (ψ) *x*=1. The inset shows the correlation between the characteristic onset frequency ω_c and the dc conductivity for *x*=0.335. The solid line represents the least-squares linear fits to BNN relation (6).

Figure 6: Angular frequency dependence of: the imaginary part Z''_S of the complex impedance for: (–) *x*=0; (ψ) *x*=1 and the imaginary part *M''* of the complex dielectric modulus for: (!) *x*=0; (ξ) *x*=1. Data points are connected to guide the eye.

Figure 7: Angular frequency dependence of the real part σ'of the complex conductivity at different temperatures between -100 and 150°C: (!) -100°C; (–) -60°C; (7) -20°C; (X) 40°C; (Λ) 80°C; (Ξ)120°C; (ψ) 150°C for *x*=0.835.

Figure 8: Dc conductivity σ_{dc} (Λ) and characteristic onset frequency ω_c (–) as function of reciprocal temperature for *x*=0.835. Solids lines represent the fit of experimental data using (4) and (5).

Figure 9: Characteristic onset frequency ω_c (–) and characteristic relaxation time τ^*_Z (ξ) as function of reciprocal temperature for *x*=0.835. Solids lines represent the fit of experimental data using (5) and (7).

Figure 10: Variation of the exponent n with temperature for x=0.835. The inset shows the temperature dependence of the ratio (–LnA/n).

Tables

Table 1: Dc conductivity σ_{dc}, characteristic onset frequency ω_c and exponent n, using (1), for different $CuFe_{1-x}Cr_xO_2$ delafossite powders at room temperature.

Table 2: Number density of Cu sites N_{Cu}, Cu- Cu distance (a-axis lattice parameter), number density of effective charge carrier density N_c using (8) and charge carrier mobility μ using (9) for different powders at room temperature.

	σ_{dc} (S.cm^{-1})	ω_c (s^{-1})	n
$CuFeO_2$:Mg	9.3×10^{-8}	2.3×10^{5}	0,92
$CuFe_{0,835}Cr_{0,165}O_2$:Mg	7.2×10^{-8}	1.8×10^{5}	0,97
$CuFe_{0,667}Cr_{0,333}O_2$:Mg	2.3×10^{-7}	3.5×10^{5}	0,89
$CuFe_{0,5}Cr_{0,5}O_2$:Mg	5.6×10^{-7}	4.8×10^{5}	0,70
$CuFe_{0,333}Cr_{0,667}O_2$:Mg	4.0×10^{-7}	2.8×10^{5}	0,66
$CuFe_{0,165}Cr_{0,835}O_2$:Mg	5.1×10^{-7}	4.0×10^{5}	0,65
$CuCrO_2$:Mg	1.4×10^{-6}	8.4×10^{5}	0,64

Table 1

	N_{Cu} (m^{-3})	a (Å) [15]	N_C (m^{-3})	μ(m^{-2}.V^{-1}.S^{-1})
$CuFeO_2$:Mg	2.19×10^{28}	3,0344	2.19×10^{27}	2.2×10^{-14}
$CuFe_{0,835}Cr_{0,165}O_2$:Mg	2.21×10^{28}	3,0268	2.21×10^{27}	1.7×10^{-14}
$CuFe_{0,667}Cr_{0,333}O_2$:Mg	2.22×10^{28}	3,0159	2.22×10^{27}	3.3×10^{-14}
$CuFe_{0,5}Cr_{0,5}O_2$:Mg	2.24×10^{28}	3,0055	2.24×10^{27}	4.5×10^{-14}
$CuFe_{0,333}Cr_{0,667}O_2$:Mg	2.26×10^{28}	2,9942	2.26×10^{27}	2.6×10^{-14}
$CuFe_{0,165}Cr_{0,835}O_2$:Mg	2.28×10^{28}	2,9826	2.28×10^{27}	3.7×10^{-14}
$CuCrO_2$:Mg	2.29×10^{28}	2,9742	2.29×10^{28}	7.7×10^{-14}

Table 2

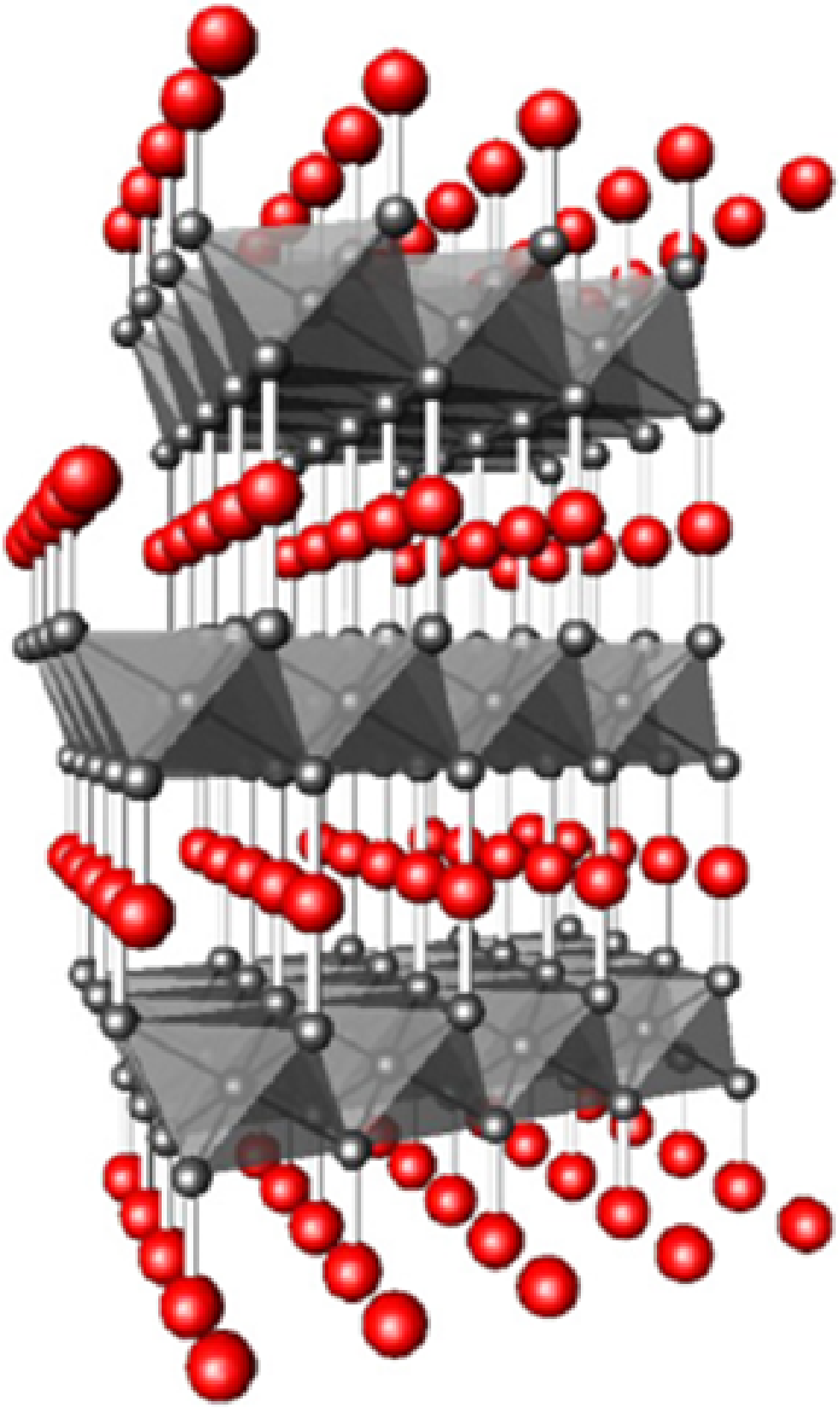

Figure 1 (figure1.jpg)

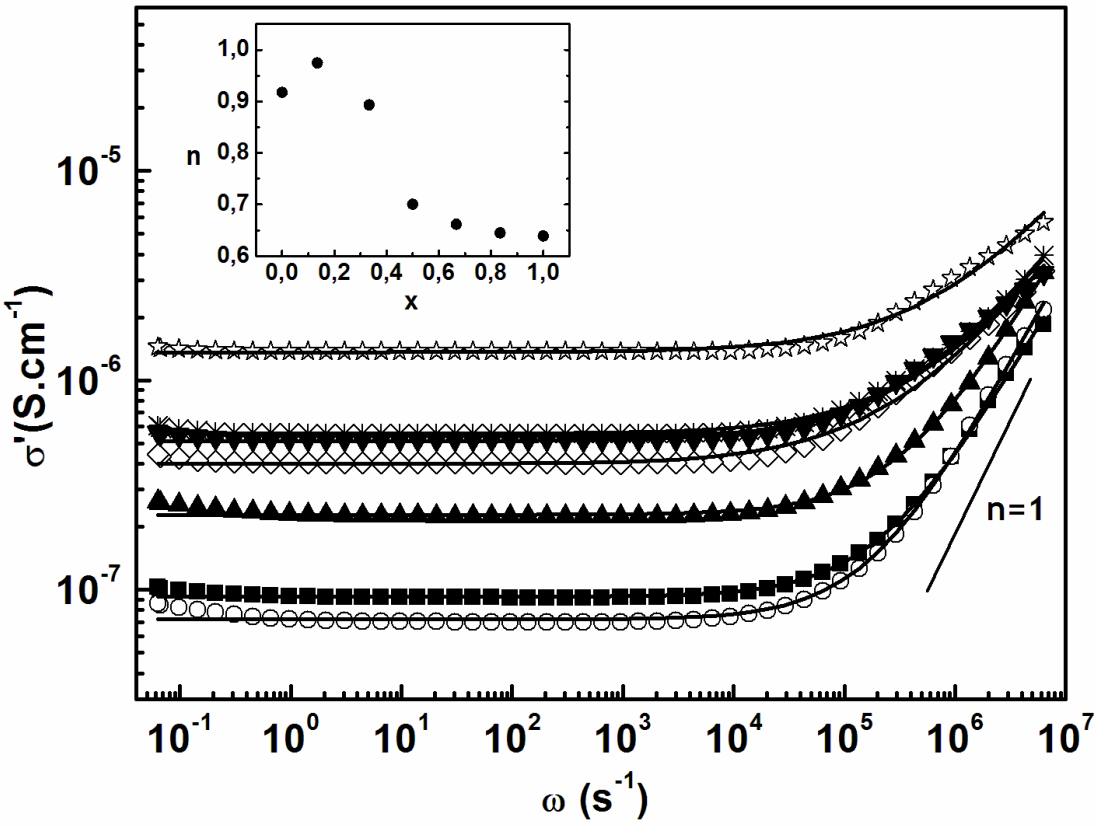

Figure 2 (figure2.TIF)

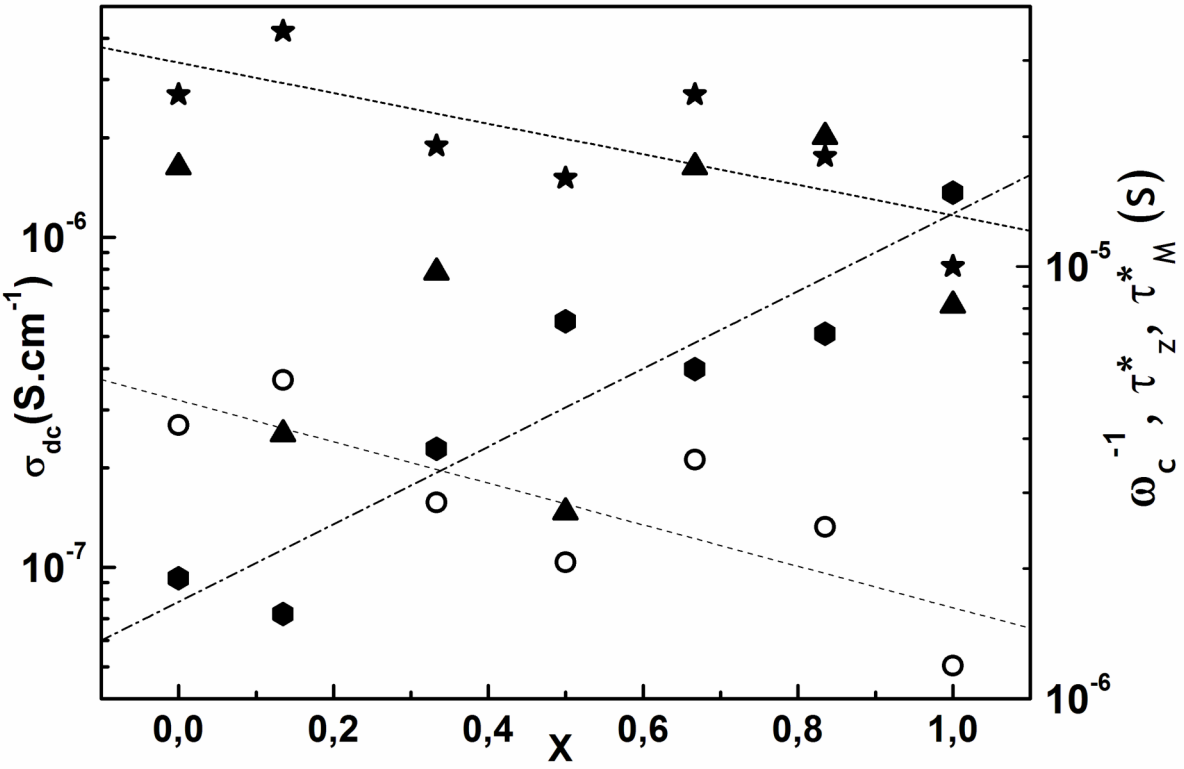

Figure 3 (figure3.TIF)

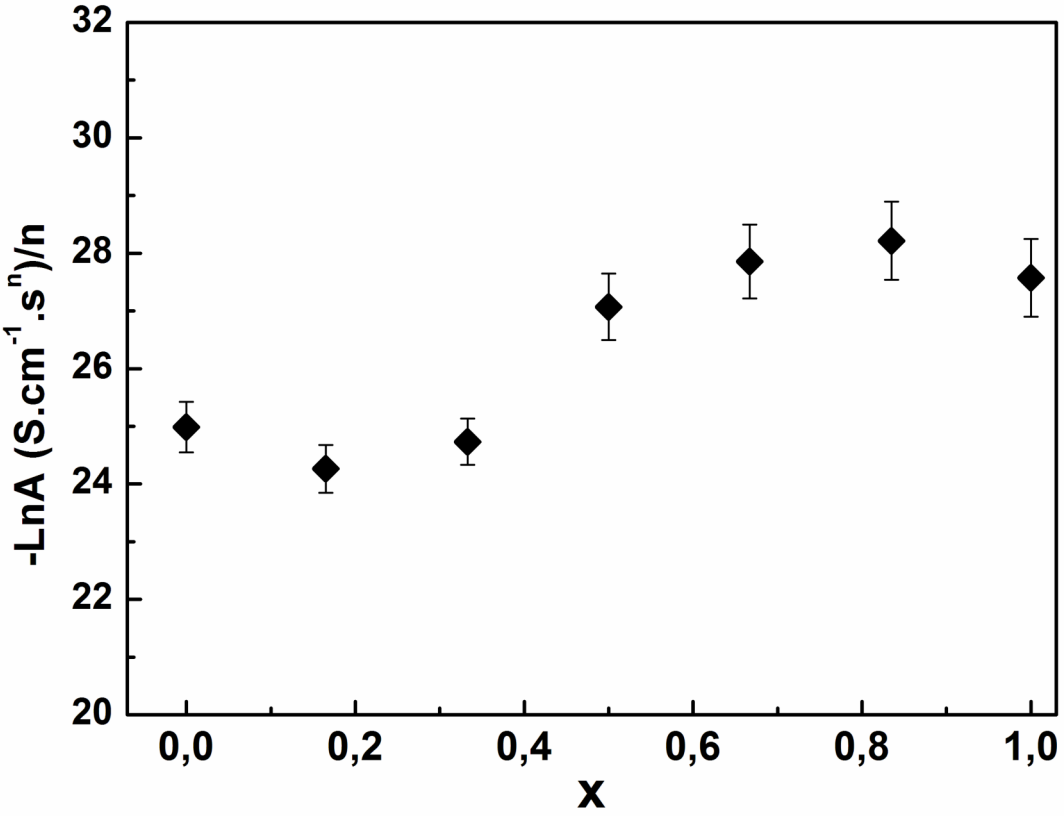

Figure 4 (figure4.TIF)

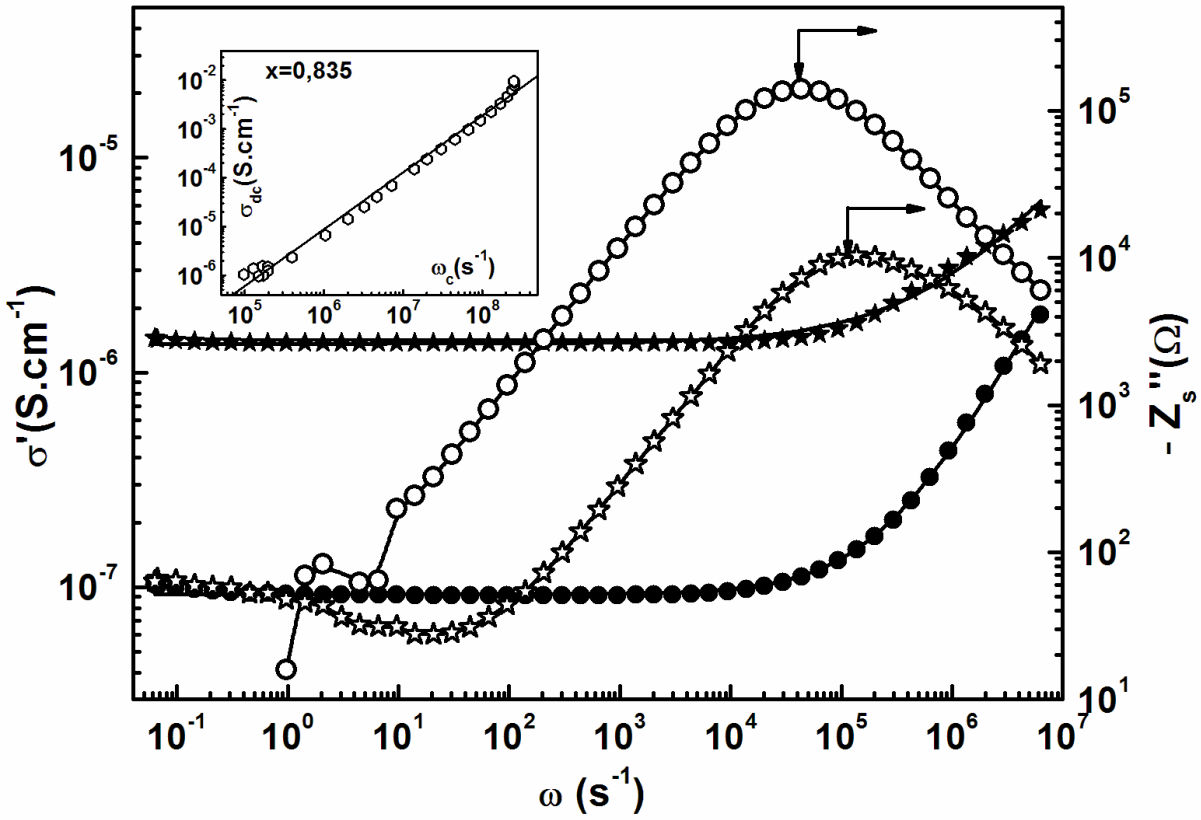

Figure 5 (figure5.TIF)

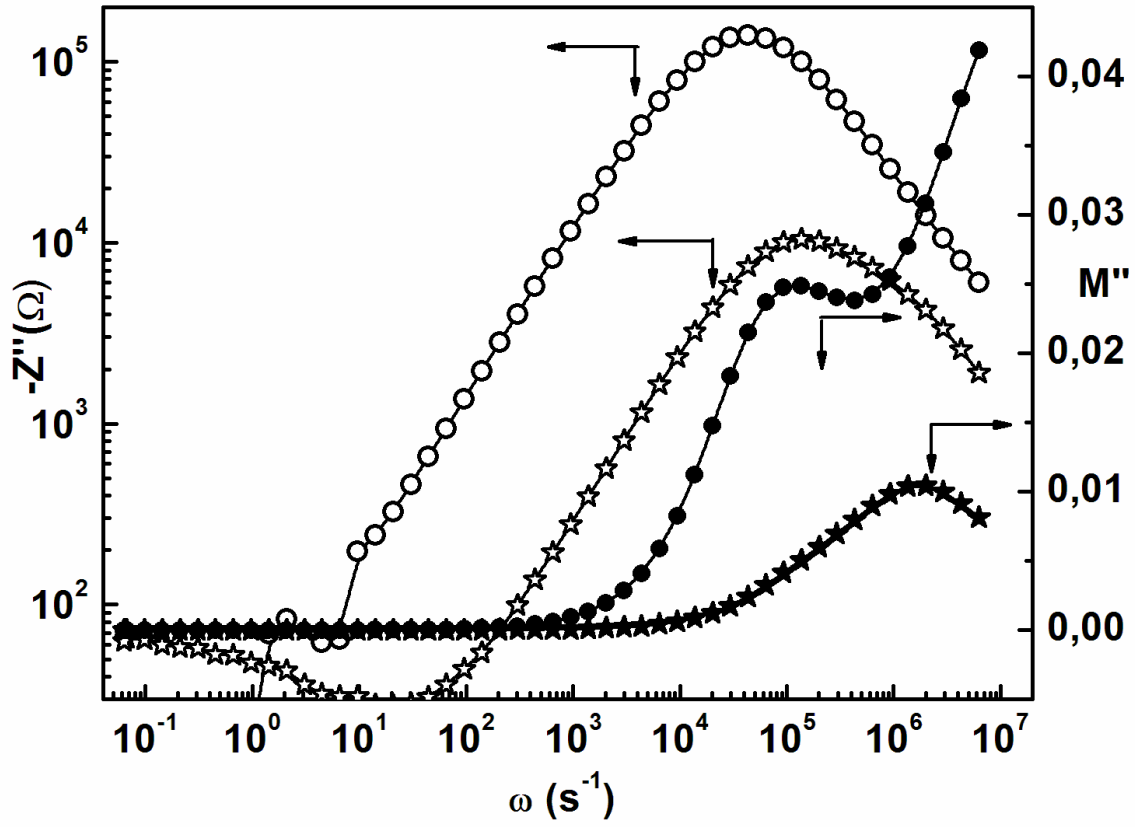

Figure 6 (figure6.TIF)

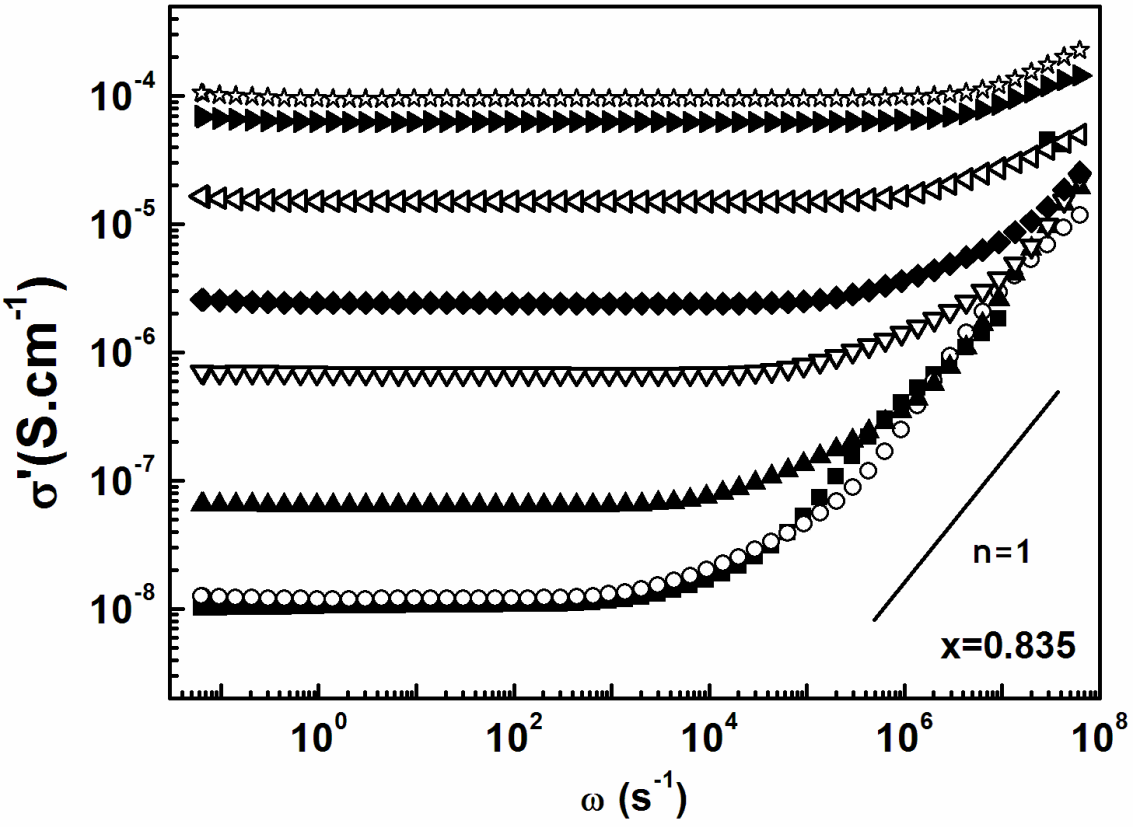

Figure 7 (figure7.TIF)

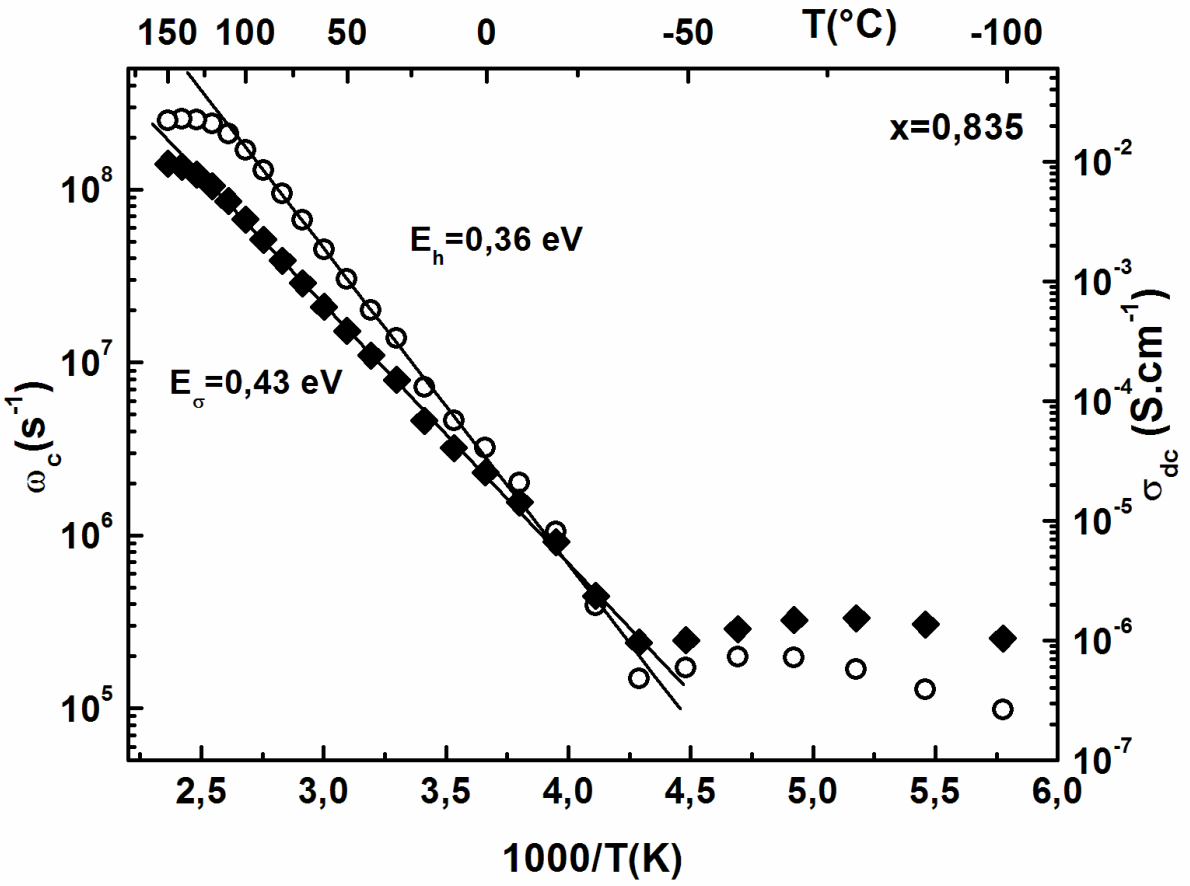

Figure 8 (figure8.TIF)

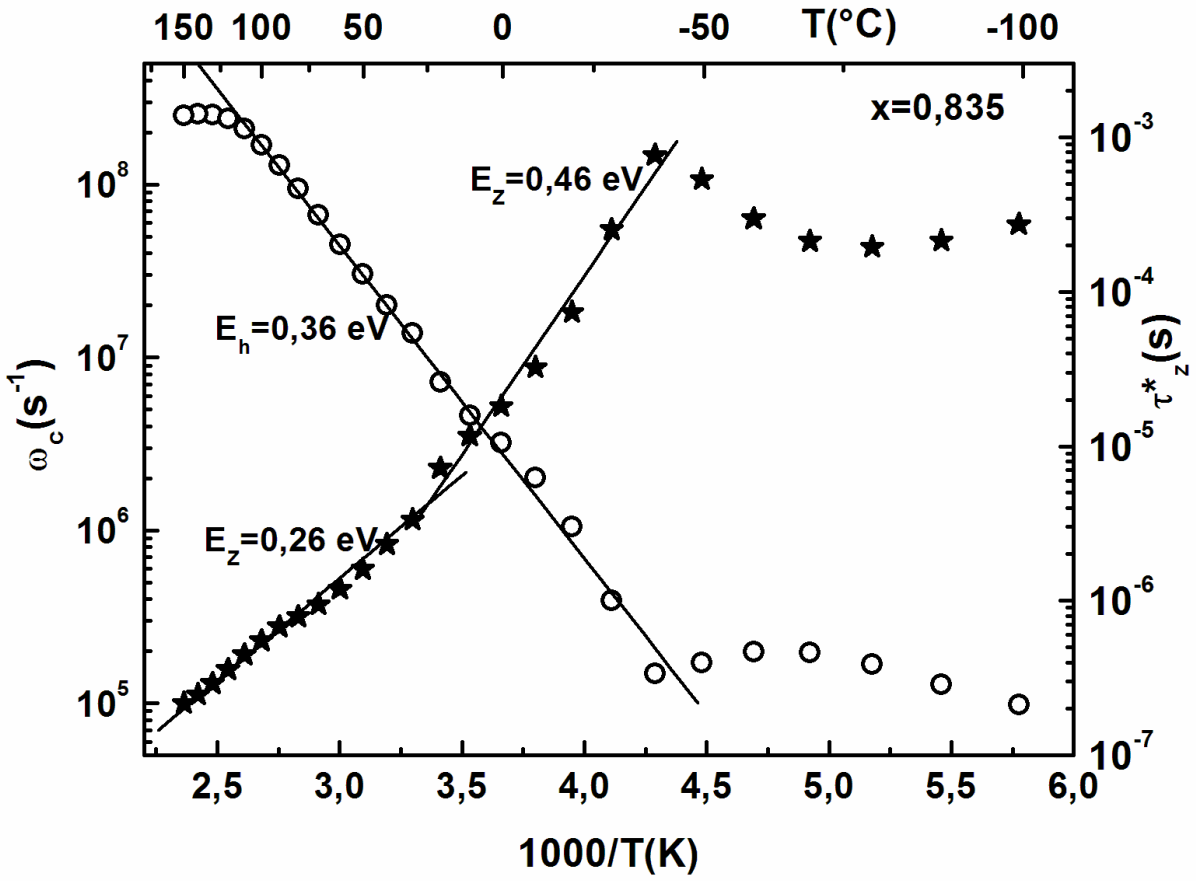

Figure 9 (figure9.TIF)

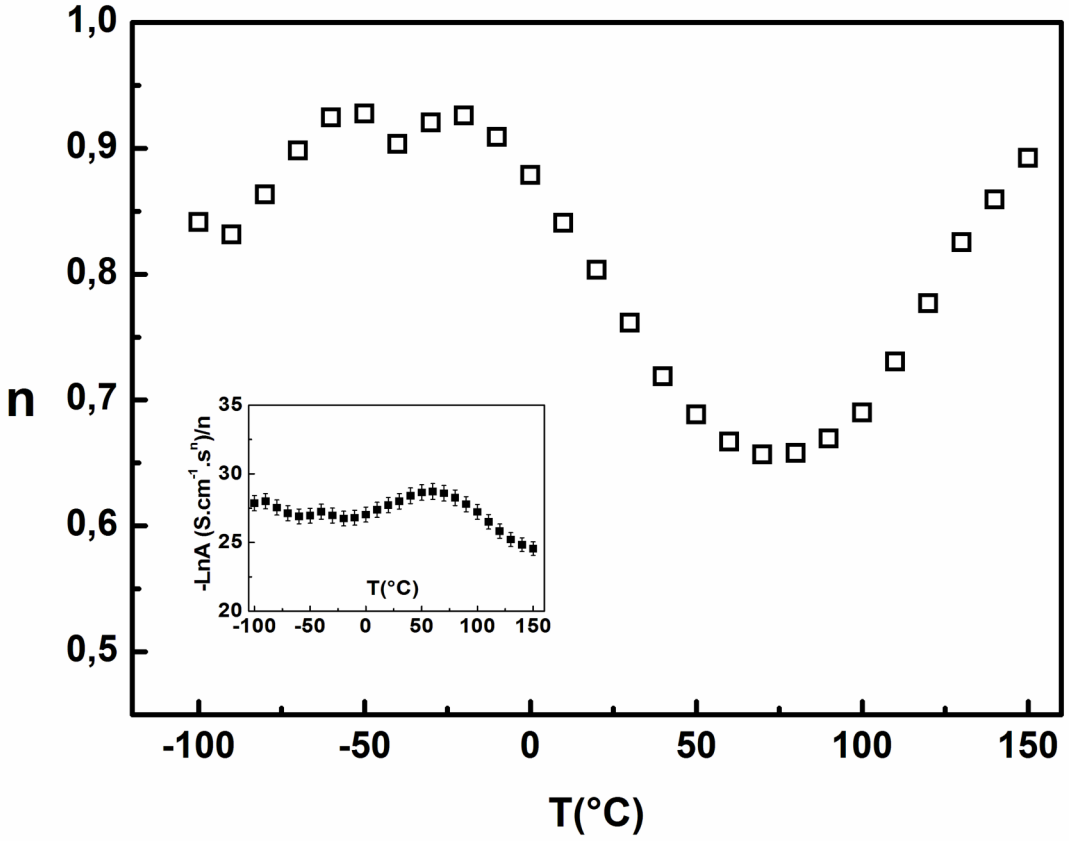

Figure 10 (figure10.TIF)